Multi-Scale MHD Analysis of LHD Plasma with Background Field Changing

K. Ichiguchi[1,2], S. Sakakibara[1,2], S. Ohdachi[1,2], B. A. Carreras[3]

[1]National Institute for Fusion Science, 322-6 Oroshi-cho, Toki 509-5292, Japan
[2]The Graduate University for Advanced Studies, SOKENDAI, 322-6 Oroshi-cho, Toki 509-5292, Japan
[3]Universidad Carlos III, 28911 Leganes, Madrid, Spain

E-mail: ichiguch@nifs.ac.jp

Abstract. The mechanism of the partial collapse observed in the experiment with the background magnetic field changing in the Large Helical Device (LHD) is numerically investigated with a nonlinear magnetohydrodynamics (MHD) simulation. Since the different time scales of the perturbations and the background field changing have to be treated simultaneously for the analysis of this plasma, a multi-scale simulation scheme is developed. The effect of the perturbation dynamics on the equilibrium pressure and rotational transform is taken into account in this scheme. The result indicates that the collapse is caused by the destabilization of an infernal-like mode due to the magnetic hill enhanced by the change of the background field. The mechanism of the reduction of the central beta observed after the partial collapse in the experiment is also analyzed in relation with the effect of the background field changing.

PACS numbers: 52.65.Kj,52.55.Hc

1. Introduction

In the design study of DEMO reactors, it is crucial to avoid collapse phenomena caused by the magnetohydrodynamics (MHD) instabilities. For this purpose, we have to identify the stability window against the instabilities in the freedom of the magnetic configuration space. In heliotron configurations, such as the Large Helical Device (LHD) [1], pressure driven modes are the most dangerous MHD instabilities. However, systematic estimation methods for the collapse boundary against the modes in the configuration space have not been established yet. The horizontal position of the vacuum magnetic axis in the major radius direction, R_{vax}, is one of the dominant control parameters concerned with the stability. In the LHD experiments, the highest average beta value of 5.1% is obtained in the configuration with $R_{vax} = 3.6$m [1]. When the magnetic axis is shifted inwardly, the magnetic hill in the vacuum configuration is enhanced, and therefore, the stability against the pressure driven mode is expected to be degraded. Hence, it is necessary to identify the collapse boundary in the inward shift of the magnetic axis to obtain the knowledge for the design of the heliotron type of DEMO.

In the LHD, an experiment called a magnetic axis swing operation was carried out to investigate the collapse boundary [2]. In the operation, the background poloidal field was changed during a discharge so that the corresponding vacuum magnetic axis position was shifted inwardly in a constant rate from $R_{vax} = 3.6$m to $R_{vax} = 3.5$m. During the discharge, a partial collapse in the core electron temperature was observed. On the other hand, no collapse was observed in the case where the corresponding vacuum magnetic axis was fixed as $R_{vax} = 3.6$m without the background field changing. Thus, in the present study, we analyze the mechanism of the partial collapse with a nonlinear MHD simulation.

In the analysis of the plasma behavior in the magnetic axis swing operation, we have to incorporate the effects of the background field changing in the simulation. The equilibrium quantities change depending on the background field changing, which affect the perturbation dynamics. Also, the nonlinear evolution of the perturbation affects the equilibrium. Therefore, the time evolution of both equilibrium and perturbed quantities should be treated simultaneously. However, the time scales of these quantities are quite different. In the magnetic axis swing discharge, the background field is changed so that R_{vax} varies by 0.1m in 2sec. On the other hand, the typical time scale of the perturbation dynamics is the Alfvén time, which is in the order of 10^{-6}sec. Therefore, we have to solve a multi-scale problem.

We have developed a simulation scheme to treat such problems including two dynamical processes with quite different time scales. Originally, we developed a scheme to analyze the LHD plasma in the beta ramp-up phase [3]. The scheme is composed of the calculations of nonlinear dynamics and three-dimensional static equilibria. In the time evolution, the equilibrium is updated every certain length of the dynamics calculation. The NORM code [4] based on the reduced MHD equations [5, 6] is used for

the analysis of the perturbation dynamics corresponding to the short time scale, and the VMEC code [7] is used for the equilibrium update corresponding to the long time scale. The deformation of the pressure profile due to the resistive pressure driven instability dynamics is incorporated in the equilibrium update. By utilizing this scheme, we showed that there exists a path toward a high beta region without a significant collapse even in the linearly unstable configuration. In this calculation, the effect of the plasma heating for the beta ramp-up was included, while the background field was kept constant.

We utilize the basic idea of the original multi-scale scheme in the analysis of the plasma with the magnetic axis swing. And we modify the scheme so that the effect of the background field changing is included and the beta value is kept constant. Recently, we analyzed the magnetic axis swing plasma by utilizing the modified multi-scale scheme and obtained a preliminary result showing a pressure collapse [8]. It was found that the growth of an infernal-like mode is accelerated by the change of the background field and the nonlinear evolution leads to the partial collapse. However, the result showed that the mode is destabilized also in the case without the background field changing, while the plasma is stable in the experiment in this case.

Thus, in the present analysis, in order to obtain a result that correlates well with the experiment, we improve the simulation procedure. First, we use a better initial condition of the pressure and the rotational transform. For the initial pressure, we use a profile similar to the experimentally observed profile. For the rotational transform, we use a nonlinearly saturated profile obtained in a preparatory calculation. Next, we improve the multi-scale scheme so as to incorporate the changes of not only the pressure but also the rotational transform due to the dynamics in the equilibrium update, while the equilibrium rotational transform was automatically determined under the no net current constraint in the recent analysis [8]. These improvements allow us to reproduce the plasma behavior closer to the experimental result, and to analyze the details of the collapse phenomena.

This paper is organized as follows. In Section 2, the multi-scale scheme is explained. Particularly, we focus on the improved points beyond the procedure explained in Ref.[8]. The details of the procedure are given. In Section 3, the simulation results are compared with the experimental results. The mechanism of the appearance and the repetition of the partial collapse is discussed. Concluding remarks are given in Section 4.

2. Multi-Scale Scheme Incorporating Background Field Changing

The main frame of the present multi-scale scheme is similar to that explained in Ref.[8]. The time evolution of the plasma is simulated in a sequence of time intervals with a fixed length. In each interval, a predictor-corrector method is employed. In the i-th interval of $t_i \leq t \leq t_{i+1}$, three dimensional equilibria are calculated at $t = t_i$ and $t = t_{i+1}$ by means of the VMEC code [7] with the corresponding background vacuum magnetic field. The toroidally averaged equilibrium quantities needed for the dynamics calculation are obtained from the VMEC equilibria and interpolated into the value at every time step of

the nonlinear dynamics calculation. Then, the time evolution of the nonlinear dynamics is calculated with the interpolated quantities by means of the NORM code. This code solves the reduced MHD equations [5, 6], which are composed of the Ohm's law, the vorticity equation and the pressure equation for poloidal flux Ψ, stream function Φ and pressure P. The flux coordinates (ρ, θ, ζ) are employed, where ρ denotes the square root of the normalized toroidal magnetic flux, and θ and ζ are the poloidal and the toroidal angles, respectively. The detail of this code is explained in Ref.[4, 8]. In this multi-scale scheme, it is essential to incorporate the change of the pressure and the rotational transform due to the dynamics as well as the change of the background field in the equilibrium calculation. In the present study, the scheme is improved mainly in the incorporation procedure of the rotational transform change from that used in Ref.[8]. Here we focus on the improvement in this section.

The first improved point is that the fixed rotational transform constraint is employed in each VMEC equilibrium calculation. In the VMEC code, we can use either fixed or free boundary condition. Furthermore, we can also use either constraint of no net toroidal current or fixed rotational transform. In the analysis of the plasma with the background field changing, the free boundary calculation is essential. Besides, in order to incorporate the change in the rotational transform due to the dynamics calculation, the fixed rotational transform constraint is desirable. However, it is difficult to obtain a good convergence for fine radial grids in the free boundary equilibrium calculation, in particular, under the fixed rotational transform constraint. Thus, in order to obtain a solution in fine grids with sufficient convergence, we run the code two times in succession. In the first run, we calculate the free boundary equilibrium with coarse grids under the no net toroidal current constraint. Here, we assume that the net toroidal current corresponding to the change of the rotational transform is too small to affect the position and the shape of the plasma boundary. In this run, the change of the background field is incorporated. In the second run, we calculate a fixed boundary equilibrium with fine grids under the fixed rotational transform constraint utilizing the boundary data obtained in the first run.

The next point is the modification of the initial condition. In order to provide the initial rotational transform, we utilize a preparatory simulation. In the present study, we assume that the initial state is a stationary state at high beta. We consider that such state results from nonlinear saturation of weak turbulence of the pressure driven modes [3]. In order to obtain such a situation, we calculate the time evolution with the vacuum axis position fixed. We employ the poloidal magnetic flux and the current density obtained in the saturation phase for the initial condition of the present study, which are denoted by $\Psi^\dagger$ and $J_\zeta^\dagger$, respectively. Then, the initial equilibrium rotational transform ι_{eq}^{ini} is obtained as

$$\iota_{eq}^{ini} = \frac{1}{\rho}\frac{d\langle\Psi^\dagger\rangle}{d\rho}, \tag{1}$$

which is used for the initial equilibrium calculation together with a specified pressure profile P_{eq}^{ini}. Here the angle bracket indicates the average over the angular variables and

the subscript of 'eq' denotes an equilibrium quantity. We utilize $J_\zeta^\dagger$ for the initial net toroidal equilibrium current density in the vorticity equation as

$$J_{\zeta eq}^{ini}(m=0) = \langle J_\zeta^\dagger \rangle, \tag{2}$$

corresponding to ι_{eq}^{ini}, where m and n are the poloidal and the toroidal mode numbers.

Final point is the specification of the rotational transform in each equilibrium calculation, which is needed for the fixed rotational transform constraint. In the predictor step, we specify the rotational transform at $t = t_i$ in the i-th interval, with utilizing the dynamics result in the previous interval, as

$$\iota_{eq,i}^{pre}(t_i) = \iota_{eq}^{ini} + \frac{1}{\rho}\frac{d\langle\tilde{\Psi}\rangle_{i-1}^{cor}(t_i)}{d\rho}, \tag{3}$$

and at $t = t_{i+1}$

$$\iota_{eq,i}^{pre}(t_{i+1}) = \iota_{eq,i}^{pre}(t_i). \tag{4}$$

under the assumption of the constant rotational transform in the predictor step. Here, the superscripts of "*pre*" and "*cor*" indicate the quantity in the predictor and the corrector steps, respectively, and the subscript of i means the quantity in the i-th interval. The variable of $\tilde{\Psi}$ denotes the poloidal magnetic flux perturbation obtained by the nonlinear dynamics calculation. In the corrector step, we use the same equilibrium quantities as in the predictor step at $t = t_i$, and therefore,

$$\iota_{eq,i}^{cor}(t_i) = \iota_{eq,i}^{pre}(t_i). \tag{5}$$

We specify the rotational transform at $t = t_{i+1}$, with utilizing the dynamics result in the predictor step, as

$$\iota_{eq,i}^{cor}(t_{i+1}) = \iota_{eq}^{ini} + \frac{1}{\rho}\frac{d\langle\tilde{\Psi}\rangle_{i}^{pre}(t_{i+1})}{d\rho}. \tag{6}$$

Corresponding to the above specification of the rotational transform, the net equilibrium toroidal current density given by eq.(2) is kept for the whole time evolution i.e., $J_{\zeta eq}(m=0)(t) = J_{\zeta eq}^{ini}(m=0)$.

The equilibrium pressure is determined in the way similar to Ref.[8]. That is, we use

$$P_{eq,i}^{pre}(t_i) = \langle P\rangle_{i-1}^{cor}(t_i), \quad P_{eq,i}^{pre}(t_{i+1}) = P_{eq,i}^{pre}(t_i) \tag{7}$$

in the predictor step, and

$$P_{eq,i}^{cor}(t_i) = P_{eq,i}^{pre}(t_i), \quad P_{eq,i}^{cor}(t_{i+1}) = \langle P\rangle_{i}^{pre}(t_{i+1}) \tag{8}$$

in the corrector step. Here $\langle P\rangle$ denotes the average part of the pressure obtained in the nonlinear dynamics calculation.

Concerning with the numerical parameters, the numbers of the radial grid in the VMEC calculation are 61 and 121 for the free and fixed boundary calculations, respectively. In the nonlinear dynamics calculation with the NORM code, the number of the radial grid is 96. The toroidal and poloidal mode numbers are chosen as $0 \le n \le 7$ and $2n - 20 \le m \le 2n + 20$, respectively. In the dynamics calculation,

we employ the dissipation parameters, $S = 1.0 \times 10^7$, $\nu = 5.0$, $\kappa_\perp = 1.0 \times 10^{-6}$ and $\kappa_\parallel = 4.0 \times 10^{-3}$ for magnetic Reynolds number, viscosity, and perpendicular and parallel heat conductivities, respectively, Here S is defined as $S = \tau_R/\tau_A$ with the poloidal Alfvén time $\tau_A = R_0\sqrt{\mu_0\rho_m}/B_0$ and the resistive diffusion time $\tau_R = \mu_0 a^2/\eta$, where B_0, R_0, a, ρ_m, μ_0, and η are the magnetic field at the magnetic axis, the major radius, the average minor radius, the mass density, the vacuum permeability, and the resistivity, respectively, and the values of $R_0 = 3.6$m, $a/R_0 = 0.1566$ and $\tau_A = 2.2 \times 10^{-6}$sec are used. The coefficients of ν, $\kappa_\perp$ and $\kappa_\parallel$ are normalized by $(a^2\rho_m)/\tau_A$, a^2/τ_A and R_0^2/τ_A, respectively. The heat source term Q is also specified in the vorticity equation so that the beta value should be constant for the given viscosity and heat conductivity in the region before the collapse. The profile and the absolute value are determined by a trial-and-error technique in the observation of the beta value over the initial several intervals. Once the source term Q is specified, the term is fixed in the whole time evolution to simulate the situation with the constant heating.

3. Simulation of Partial Collapse

In the magnetic axis swing experiment [2], the background field was changed so that the corresponding vacuum magnetic axis was shifted from $R_{vax} = 3.6$m at $t = 1.02$s to $R_{vax} = 3.5$m at $t = 3.02$s in the LHD configuration with $\gamma_c = 1.20$. The change rate of the R_{vax} is 0.05m/sec. Here, γ_c is the pitch parameter of the helical coils [10]. In the discharge, the neutral beams were applied continuously. The profiles of the electron temperature and the electron density were observed as functions of the major radius, R, on the mid plane of a horizontally elongated cross section by means of the Thomson scattering system. By utilizing the data of the electron temperature and the density, and assuming that the ion temperature is equal to the electron temperature, we can evaluate the pressure profile and identify the peak position of the profile, R_{peak}. This peak position can be recognized to coincide with the magnetic axis position. We evaluate the maximum beta value around the peak position as the central beta, β_0.

Figure 1 shows the time evolution of β_0 and R_{peak} together with R_{vax} in the experiment. A partial collapse is observed after $t = 2.200$s. Figure 2 shows the pressure profiles at $t = 2.200$s and 2.266s normalized by the magnetic pressure. The central beta is dropped from $\beta_0 = 5.6\%$ at $t = 2.200$s to $\beta_0 = 4.6\%$ at $t = 2.266$s. Furthermore, the peak position is shifted inwardly from $R_{peak} = 3.71$m at $t = 2.200$s to $R_{peak} = 3.61$m at $t = 2.266$s. On the other hand, R_{vax} changes much more slowly as shown in Fig.1. Therefore, the observed inward axis shift during the collapse is much larger than the shift due to the background field changing. Figure 1 also shows the time evolution of the $(m, n) = (2, 1)$ component of the magnetic fluctuation. The substantial fluctuation appears accompanied by the occurrence of the partial collapse. After the partial collapse, β_0 gradually decreases in average in spite of the continuous heating as shown in Fig.1. Some small sudden drops of β_0 also appear in the phase. The $(m, n) = (2, 1)$ magnetic fluctuation is still detected continuously.

By applying the multi-scale scheme, we analyze these behaviors of the plasma in the magnetic axis swing experiment. In this analysis, we change the background magnetic field linearly so that $R_{vax} = 3.60$m at $t = 7500\tau_A$ and $R_{vax} = 3.50$m at $t = 307500\tau_A$. The change rate of the R_{vax} is 0.15m/sec, which is three times larger than that in the experiment. We employ this large change rate to reduce the computation time. As an initial equilibrium pressure P_{eq}^{ini}, the profile close to that experimentally observed at $t = 2.200$s is employed, which is shown by the solid line in Fig.2. The initial equilibrium rotational transform ι_{eq}^{ini} is obtained by utilizing the preparatory simulation with $R_{vax} = 3.55$m, as discussed in Section 2. The profiles of P_{eq}^{ini} and ι_{eq}^{ini} are plotted as functions of ρ in Fig.3. In the time evolution, the length of one interval is $7500\tau_A$, corresponding to 16.5msec. In each interval, we follow the the nonlinear dynamics for 500000 steps with the time step of $1.5 \times 10^{-2}\tau_A$. We assume a fixed heat source of $Q = Q_0(1-\rho^2)^{50}$ to keep the beta value constant. For comparison, we also calculate the time evolution of the case with R_{vax} fixed to 3.60m without the background field changing under the same condition.

Figure 4 shows the time evolution of the kinetic energy of the $n = 1$ component, E_k, which is defined as

$$E_k = \frac{1}{2}\int \sum_m |\nabla\Phi_{m1} \times \nabla\zeta|^2 dV, \tag{9}$$

where dV denotes the volume integral in the plasma region and the subscripts of Φ mean the mode numbers. In the case with the background field changing, the $n = 1$ mode is destabilized around $t = 41500\tau_A$, and then, this mode dominantly grows. The growth rate increases in the time evolution and the mode is saturated about $t = 187500\tau_A$. Figure 4 also shows the time evolution of the central beta $\beta_0 = 2\mu_0 P_0/B_0^2$, where P_0 is the pressure at the magnetic axis. In the saturation of E_k, β_0 drops abruptly, which corresponds to the partial collapse observed in the experiment. On the other hand, in the case without the background field changing, the plasma is marginally stable in the whole time range. Thus, the situation that the plasmas are stable and unstable in the cases without and with the change of the background field, respectively, is reproduced in this simulation, which corresponds to the experimental result.

In order to understand the characteristics of the mode triggering the partial collapse, we plot the profile of the $n = 1$ component of the stream function at $t = 157500\tau_A$ in Fig.5. The $(m, n) = (2, 1)$ component is dominant and peaked as is usually seen in the profile of the interchange mode. However, the peak position of the component is deviated from the position of the $\iota = 1/2$ surface. Furthermore, the sideband components have the same sign and have amplitude comparable to the dominant component. These properties indicate that the mode is like an infernal mode [11, 12] rather than an interchange mode. Therefore, the partial collapse is caused by the saturation of the infernal-like mode, of which the dominant component is the $(m, n) = (2, 1)$ component. The reason why this mode is dominantly excited rather than interchange modes is that the rotational transform is close to 1/2, the magnetic shear is weak and the pressure gradient is steep in the vicinity of the magnetic axis, as shown in Fig.3. The mode numbers of the

dominant component agree with those of the magnetic fluctuation that was observed in the experiment accompanied with the partial collapse. Since the infernal mode is a pressure driven mode, the destabilization is affected by the magnetic hill. Figure 6 shows the change of V'' in the time evolution, which is the second derivative of the plasma volume with respect to the toroidal magnetic flux. The magnetic hill is enhanced at $t = 322500\tau_A$ compared with that in the initial equilibrium. This is attributed to the inward shift of the magnetic axis brought by the background field changing. Thus, the infernal-like mode is destabilized and the growth is accelerated by the enhancement of the magnetic hill during the time evolution.

In Fig.4, the time evolution of the poloidal component of the perturbed magnetic field at the plasma edge, $B_{\theta 2,1} = \nabla\zeta \times \nabla\tilde{\Psi}_{21} \cdot \nabla\theta$, is also plotted in the linear scale for the comparison with the experimental result shown in Fig.1. The perturbed field exceeds the value of 10% of its maximum value at $R_{vax} = 3.54$m. This R_{vax} can be recognized as the value at the mode appearance, which agrees well with the experimental result.

The repetition of the partial collapse is also obtained in the simulation. As shown in Fig.4, the kinetic energy of the $n = 1$ component decreases after the first saturation and reaches a minimum value at $t = 1875000\tau_A$. The kinetic energy increases again and reaches the second saturation. This repetition of the increase of the kinetic energy causes the repetition of the pressure collapse. The central beta decreases during the first collapse and reaches a minimum value at $t = 202500\tau_A$. Then, the central beta recovers and reaches a maximum value at $t = 255000\tau_A$. Figure 7 shows the $\langle P \rangle$ profiles at the time when the central beta reaches the minimum and the maximum values in the repetition. The maximum β_0 after the first collapse is lower than that just before the first collapse, which is also seen in Fig.4.

Figures 8 and 9 show the time evolution of the bird's eye view of the pressure, the stream function, and the flow pattern at the $\zeta = 0$ cross section. We can understand the detail of the repetition of the collapse by means of the figures, including the decrease of the beta. Before the first collapse, the pressure has a conic profile in the flux coordinates as shown in Fig.8(a). Since the $m = 2$ component is dominant in the infernal-like mode as shown in Fig.5, four vortices grow as shown in Fig.9(d). The vortices spread to the vicinity of the magnetic axis as shown in Fig.9(a), and the convection due to the vortices carries the core pressure to the outside. As a result, the central beta is decreased by the convection and the profile is deformed into the elliptic shape simultaneously as shown in Fig.8(b). Since the decrease of the central beta reduces the driving force of the infernal-like mode, the convection is suppressed after the collapse, as shown in Figs.9(b) and 9(e), and the kinetic energy is decreased as shown in Fig.4. On the other hand, since the continuous heating is incorporated in this analysis, the central beta is increased again as shown in Fig.8(c). Simultaneously, the $m = 2$ deformation becomes small because of the mode suppression. When the beta value reaches the marginal value, the mode is excited again as shown in Figs.9(c) and 9(f). In the second saturation of the mode, the collapse occurs again as shown in Fig.9(d). In the time evolution, the central beta reaches the minimum with a certain time delay after the kinetic energy reaches the maximum in

the collapses as shown in Fig.4. This delay is attributed to the fact that substantial convection remains after the kinetic energy reaches the maximum and the convection continues to reduce the central beta for a while.

Since the magnetic hill is enhanced continuously due to the background field changing, the threshold beta of the mode excitation is decreased in the time evolution. Therefore, in the simulation, the second collapse occurs at the lower beta value than the first collapse as shown in Figs.4 and 7. This result allows us to understand the mechanism of the gradual decrease of β_0 after the partial collapse in the experiment. The continuous $(m, n) = (2, 1)$ magnetic fluctuation shown in Fig.1 indicates that the mode is excited successively even after the partial collapse, which can cause other small collapses. The small sudden drops of β_0 are also considered to indicate the successive occurrence of the small collapses. Therefore, the successive collapses under the decrease of the threshold beta gradually degrades the central beta in average.

Figure 7 also shows that the position of the magnetic axis is shifted inwardly after the first collapse at $t = 202500\tau_A$. This inward axis shift corresponds to the decrease of R_{peak} observed in the experiment shown in Figs.1 and 2. As shown in Fig.7, the axis is shifted outwardly after the recovery of the beta value at $t = 255000\tau_A$, and then, shifted inwardly again after the second collapse at $t = 322500\tau_A$. Therefore, this axis shift is not directly caused by the background field changing. On the contrary, the direction of the shift depends on whether the central beta decreases or increases. Hence, the axis shift is due to the change of the Shafranov shift of the plasma, which is caused by the partial collapses through the change of the central beta. Thus, the mechanism of the inward shift observed after the collapse shown in Fig.1 is attributed to the reduction of the Shafranov shift.

4. Concluding Remarks

The LHD plasma with the background magnetic field changing, which corresponds to the magnetic axis swing experiment, is numerically analyzed with the multi-scale simulation scheme. In this scheme, the time evolutions of the equilibrium and the perturbation in different time scales are simultaneously treated. The changes of the pressure and the rotational transform due to the perturbation dynamics are reflected in the equilibrium evolution. Furthermore, in the present study, we employ the pressure profile close to the profile observed in the experiment just before the partial collapse and the rotational transform obtained in the nonlinearly saturated state of a preparatory simulation for the initial condition. By applying the scheme, we obtain the time evolutions with a partial collapse of the plasma pressure in the case with the background field changing and with no excitation of instabilities in the case without the background field changing, as observed in the experiment. The simulation results allow us to understand the observed feature of the partial collapse in the following way.

First, the partial collapse is caused by the infernal-like mode. This is due to the fact that the magnetic shear is weak and the pressure gradient is steep in the vicinity of the

magnetic axis in the configuration treated in the present analysis. The enhancement of the magnetic hill due to the background field changing destabilizes the mode and accelerates the growth. The convection in the nonlinear saturation causes the sudden drop of the core pressure. Second, the observation of the $(m, n) = (2, 1)$ magnetic fluctuation is due to the fact that the the dominant component of the mode has the same mode numbers. Since the rotational transform is close to 1/2 in the vicinity of the magnetic axis, the $(m, n) = (2, 1)$ infernal-like mode is dominantly destabilized. It would be interesting to compare the mode structure with the experimental data. In LHD, the systems of Soft X-ray and ECE are equipped. However, the measurement was not successfully carried out in this experiment. Third, the abrupt inward shift of the magnetic axis observed just after the partial collapse is found to be the reduction of the Shafranov shift. The decrease of the central beta by the partial collapse reduces the shift. Therefore, the time scale of the shift is much faster than the change rate of the background field changing. Fourth, the repetition of the partial collapse can be caused by the continuous heating. The subsequent collapse occurs at a lower beta value than the former collapse, because the threshold beta of the mode excitation is reduced by the magnetic hill enhancement due to the background field changing. As a result, the central beta value decreases in average after the first partial collapse in spite of the continuous heating. Similar repetition of the partial collapse is numerically obtained in the analysis of the Heliotron E plasma without the background field changing [13].

Thus, the present analysis explains the experimental results qualitatively. However, there remain quantitative differences. Firstly, there is a difference in the amount of the central beta reduction, $\Delta\beta_0$, in the partial collapse. In the experiment, $\Delta\beta_0$ is about 1% as shown in Fig.2, while $\Delta\beta_0 = 0.67\%$ in the simulation as shown in Fig.7. One candidate to obtain such large $\Delta\beta_0$ as in the experiment would be the implementation of the diamagnetic flow in the simulation. In the sawtooth simulation in a tokamak, the diamagnetic effect flow brings a large drop of the temperature in the repetition of the crash [14]. Similar effect is expected in the pressure driven modes.

Next, in order to compare the events after the first collapse more precisely, the number of the repetition should be identified by the simulation. In the present simulation, only two collapses are obtained in the whole time range, while there is the possibility that more small collapses occur in the experiment. The number of the repetition in the simulation depends on the change rate of the background field. The change rate in the simulation is three times larger than in the experiment. For the identification of the repetition number, it is necessary to employ the same change rate as that in the experiment and to follow the time evolution with three times more time steps. The computation time is dominantly consumed in the dynamics calculation. In the typical calculation, it took 5 hours for one interval of the NORM calculation by using 8 nodes each of which has 32 CPU's. We need to improve the NORM code so as to accelerate the calculation. These improvements are considered in future works.

Acknowledgments

This work was supported by budget NIFS13KNST053 of the National Institute for Fusion Science (NIFS) and Grant-in-Aid for Scientific Research (C) 22560822 from the Japan Society for Promotion Science. Super computers, Plasma Simulator in NIFS, and Helios in the Computational Simulation Center of the International Fusion Energy Research Center (IFERC-CSC), were utilized for the numerical calculations. One of the authors (B. A. C.) gratefully acknowledge support of this work by the "Catedras de Excelencia" at Universidad Carlos III de Madrid.

References

[1] Komori A et al., 2010 *Fusion Sci. Tech.* **58** 1.
[2] Sakakibara S et al. Proc. 23rd Fusion Energy Conf. Oct.11-16, 2010, Daejeon, EXS/P5-13.
[3] Ichiguchi K and Carreras B A 2011 *Nucl. Fusion* **51** 053021.
[4] Ichiguchi K et al. 2003 *Nucl. Fusion* **43** 1101.
[5] Strauss H R 1980 *Plasma Phys.* **22** 733.
[6] Green J M and Johnson J L 1961 *Phys. Fluids* **4** 875.
[7] Hirshman S P et al. 1986 *Comp. Phys. Comm.* **43** 143.
[8] Ichiguchi K and Carreras B A 2013 *Plasma Phys. Control. Fusion* **55** 014009.
[9] Nakamura Y et al. 1996 *J. Comp. Phys.* **128** 43.
[10] Ichiguchi K et al. 1996 *Nucl. Fusion* **36** 1145.
[11] Manickam J et al. 1987 *Nucl.Fusion* **27** 1461.
[12] Charlton L A et al. 1989 *Phys. Fluids* **B1** 798.
[13] Carreras B A et al. 1998 *Phys. Plasmas* **5** 3700.
[14] Halpern F D et al. 2011 *Phys. Plasmas* **18** 102501.

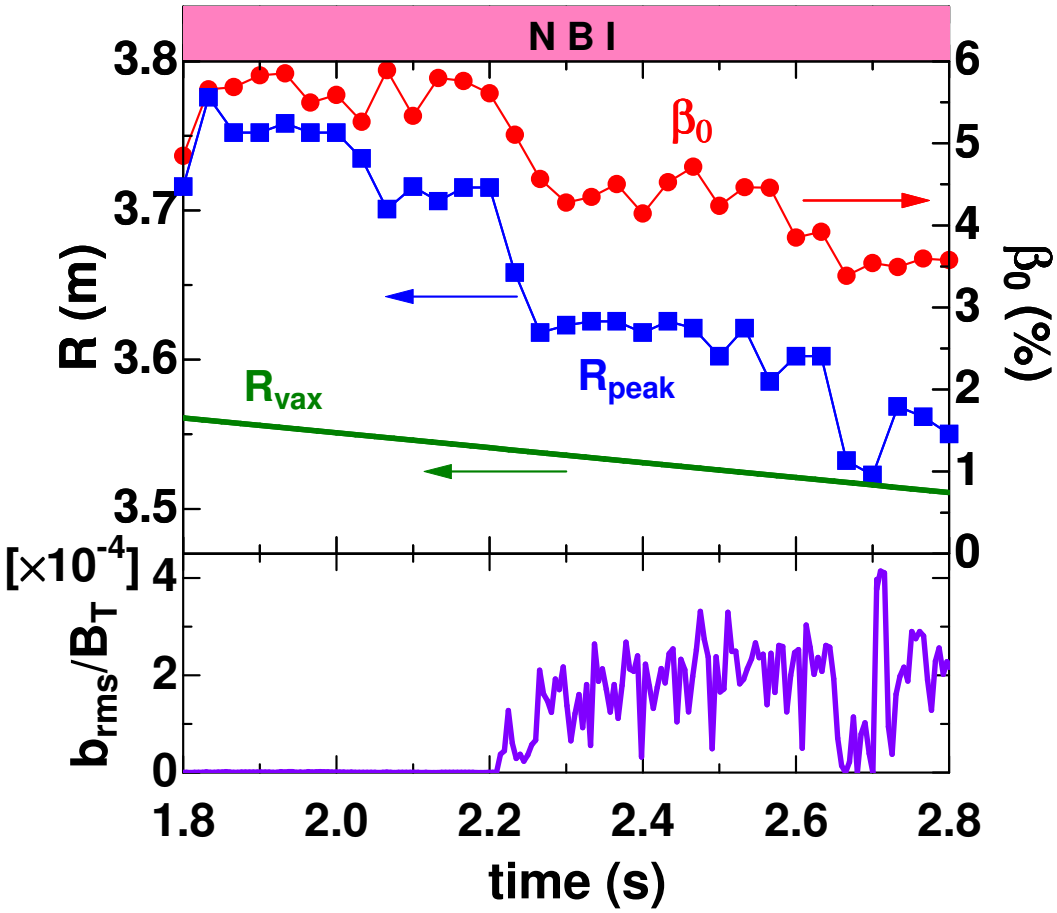

Figure 1. Time evolution of β_0 (red circle), R_{peak} (blue square) and R_{vax} (green solid line) in the magnetic axis swing experiment in LHD (#87400) are plotted in the upper graph. Time evolution of the $(m, n) = (2, 1)$ magnetic fluctuation normalized by the operational toroidal field at R_{vax}, B_T, is also plotted in the bottom graph. The neutral beams were applied continuously.

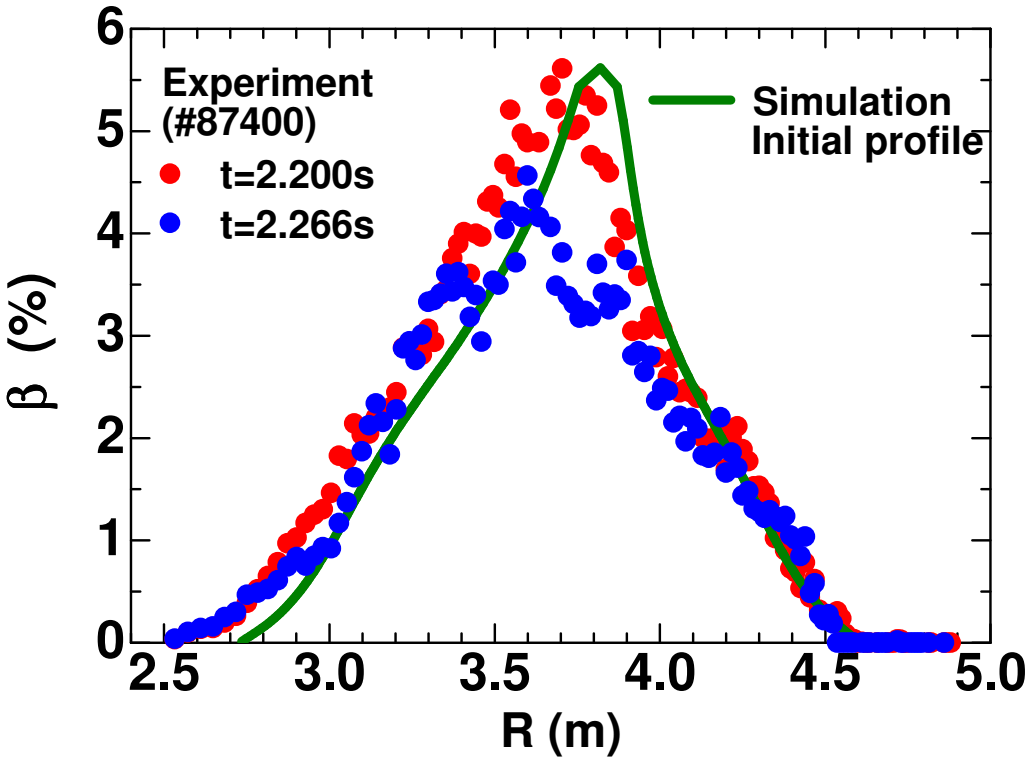

Figure 2. Profiles of the pressure normalized by the magnetic pressure observed at $t = 2.200$s (red dots) and $t = 2.266$s (blue dots) in the magnetic axis swing experiment in LHD (#87400) and the initial pressure in the present numerical simulation P_{eq}^{ini} (solid line) as the functions of the major radius R(m) in the horizontally elongated cross section.

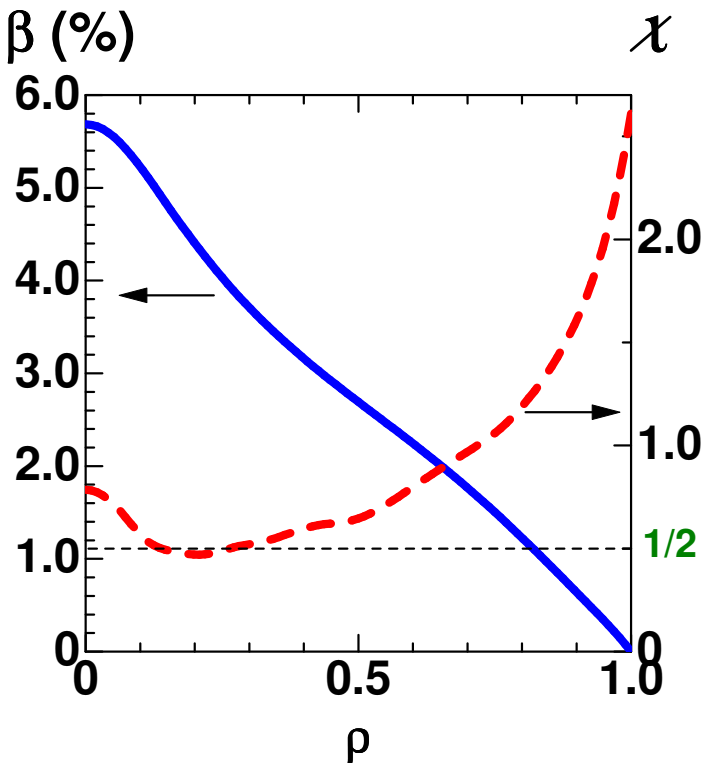

Figure 3. Initial profiles of pressure P_{eq}^{ini} (solid lines) and rotational transform ι_{eq}^{ini} (dashed lines) in the flux coordinates.

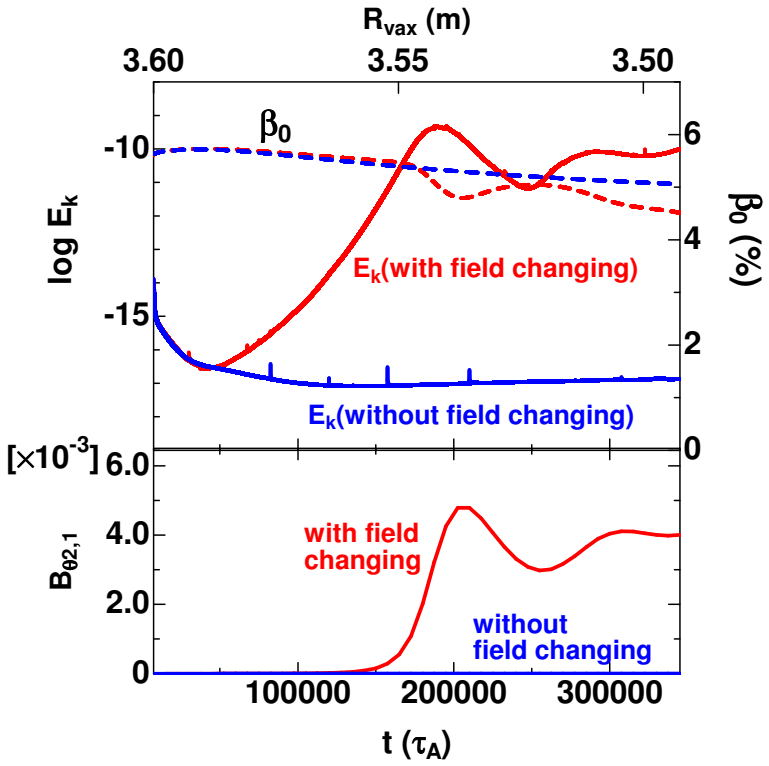

Figure 4. Time evolution of kinetic energy (E_k, solid lines) of the $n = 1$ component of the perturbation and central beta (β_0, dashed lines) in the upper graph and poloidal component of the perturbed magnetic field at the plasma edge ($B_{\theta 2,1}$) in the bottom graph in the cases with (red) and without (blue) the background field changing.

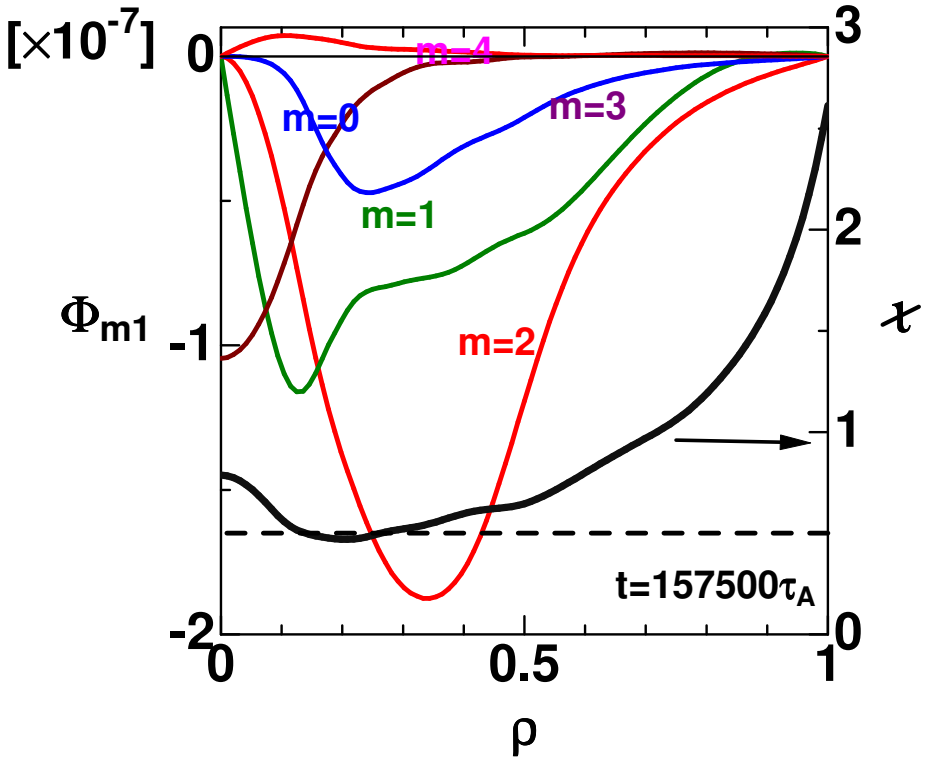

Figure 5. Mode structure of $n = 1$ stream function at $t = 157500\tau_A$ in the background field changing.

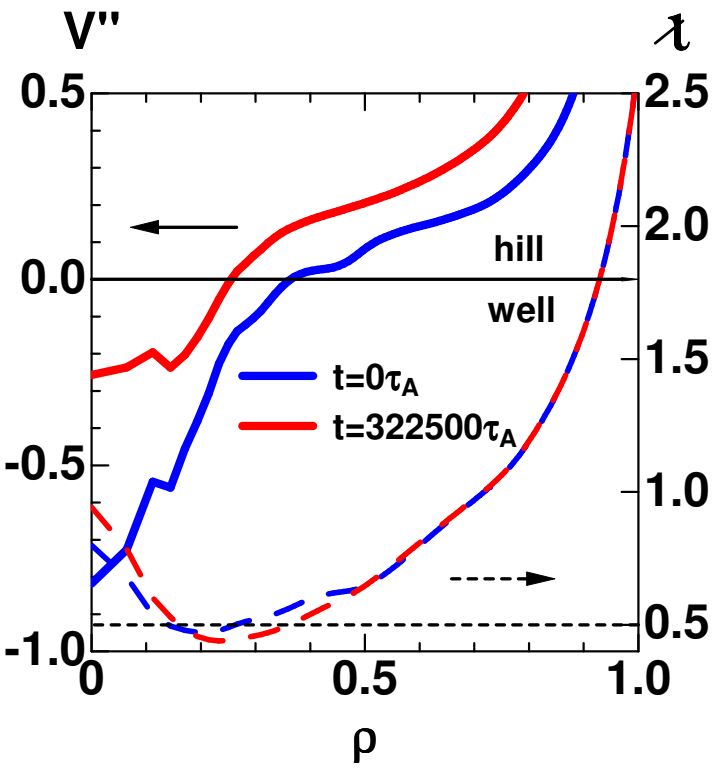

Figure 6. Variation of the profiles of V'' (solid lines) and rotational transform (dashed lines) in the background field changing.

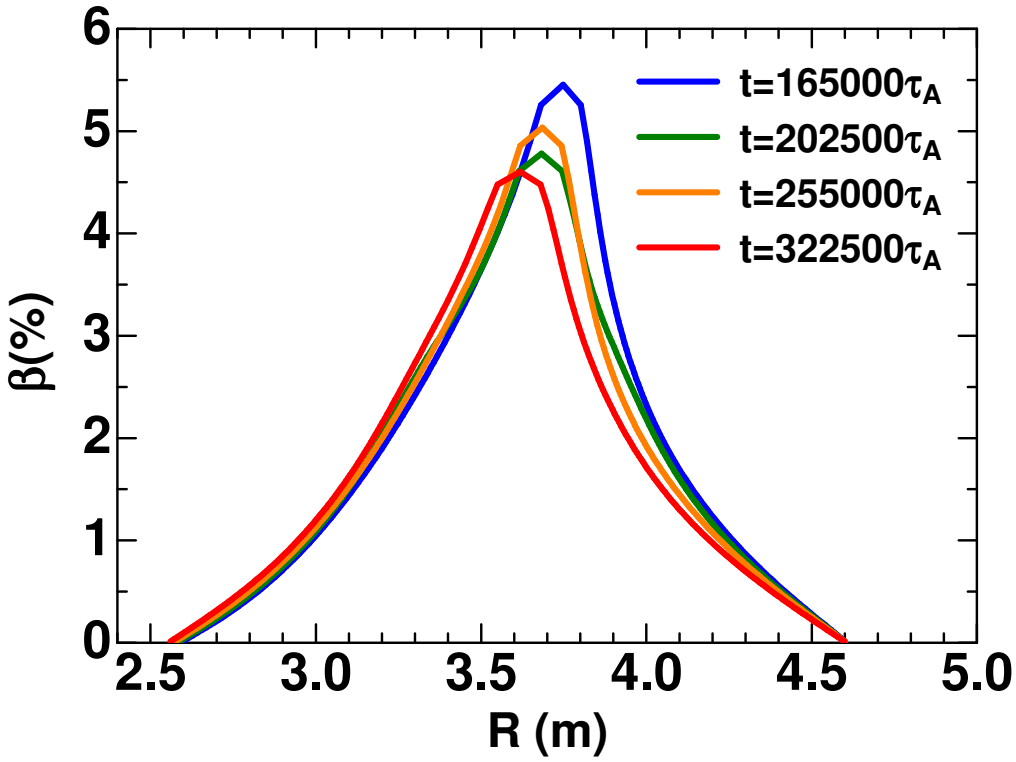

Figure 7. Profiles of $\langle P \rangle$ at $t = 165000\tau_A$, $t = 202500\tau_A$, $t = 255000\tau_A$ and $t = 322500\tau_A$ in the background field changing.

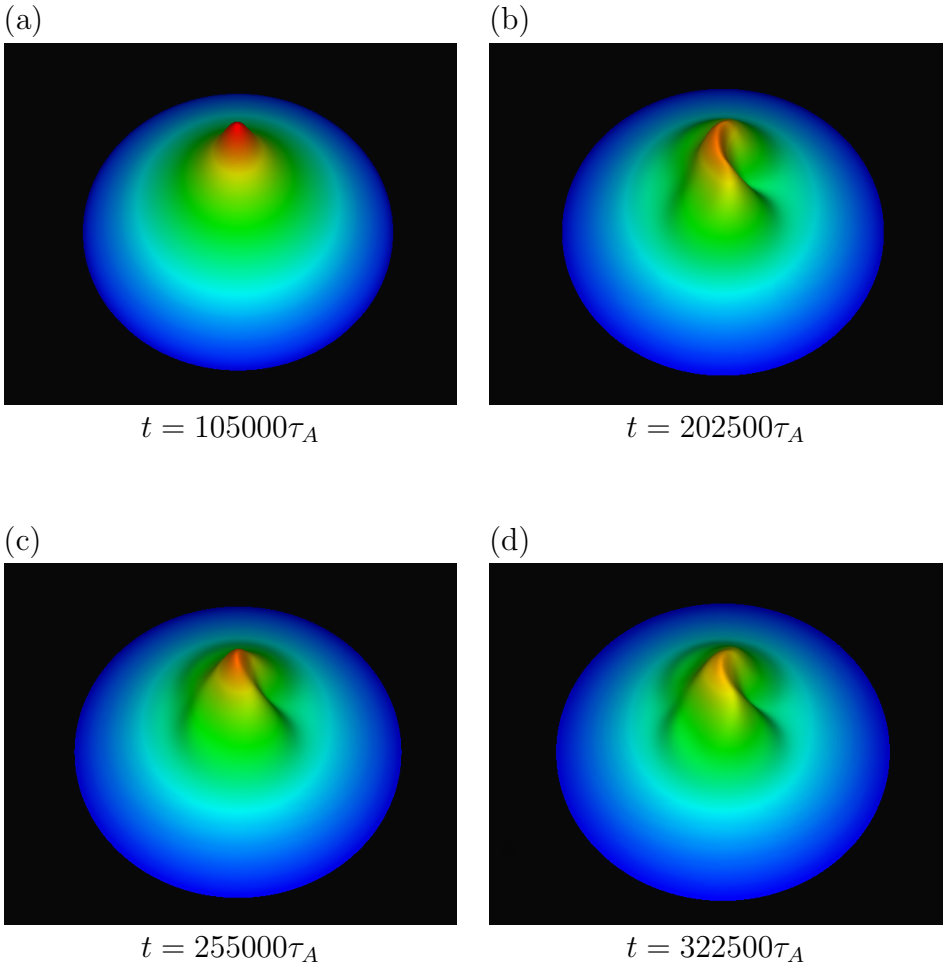

Figure 8. Bird's eye view of total pressure in the $\zeta = 0$ plane at (a) $t = 105000\tau_A$, (b) $t = 202500\tau_A$, (c) $t = 255000\tau_A$ and (d) $t = 322500\tau_A$ in the background field changing.

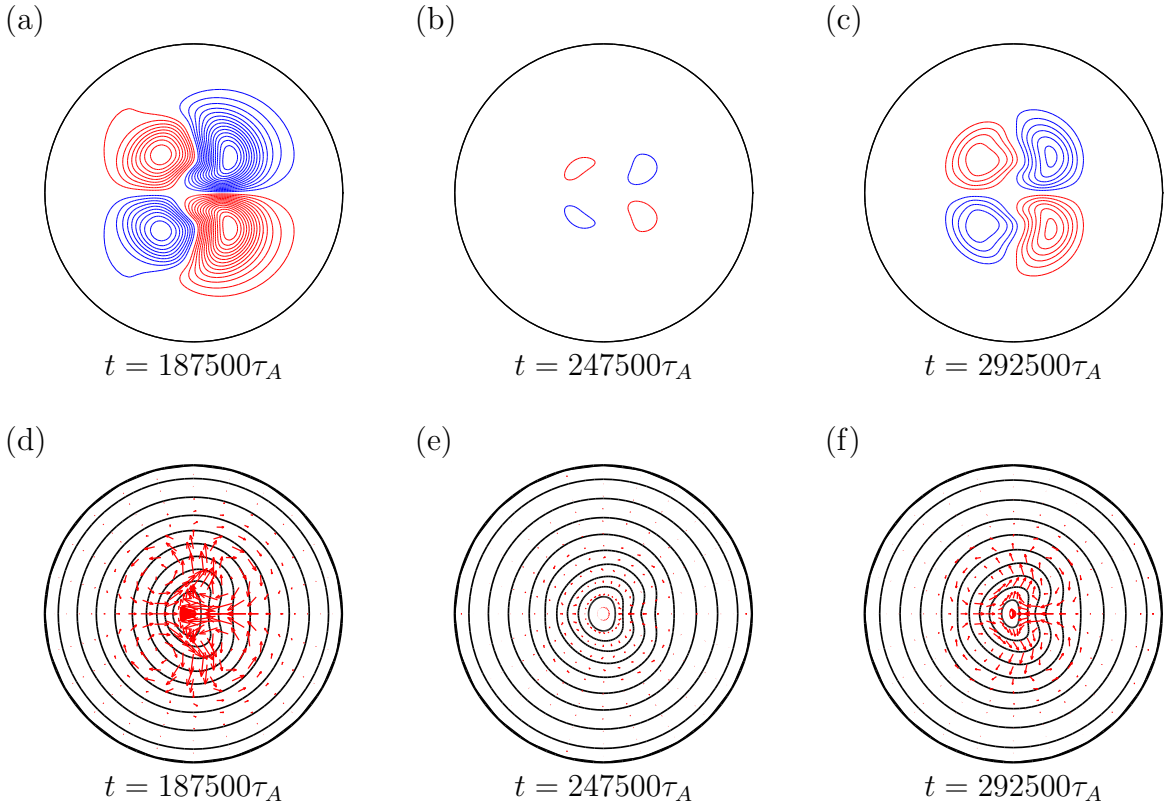

Figure 9. Stream function (upper row) and flow pattern and pressure contours (bottom row) in the $\zeta = 0$ plane at (a), (d) $t = 187500\tau_A$, (b), (e) $t = 247500\tau_A$ and (c), (f) $t = 292500\tau_A$ in the background field changing.